AIAA JOURNAL
Vol. 32, No. 10, October 1994

Interaction of a Streamwise Vortex with a Thin Plate: A Source of Turbulent Buffeting

Alejandro Mayori* and Donald Rockwell†
Lehigh University, Bethlehem, Pennsylvania 18055

The three-dimensional interaction of a streamwise vortex with a thin plate (simulated tail or fin) is investigated experimentally using high-image-density particle image velocimetry, which allows determination of the instantaneous streamline patterns and distributions of vorticity over entire planes of the flow. These representations of the flow reveal that the vortex-plate encounter generates a new type of vortex splitting, leading to two smaller-scale concentrations of streamwise vorticity. Their trajectories rapidly diverge from the plane of symmetry of the plate. Details of this encounter process are interpreted using instantaneous values of circulation, two-dimensional vorticity correlation functions, and length scales of the vorticity field.

Nomenclature

C = root chord of wing that generates vortex, mm
D = diameter (time mean) of incident vortex measured between peak values of swirl velocity V_θ, mm
f = frequency, c/s
L = length of plate, mm
L_i = length scale of vortical structures in i direction, mm
R_ω = vorticity correlation function
$\underline{r}$ = tangent to curve along which circulation is evaluated, mm
t = thickness of plate, mm
U = freestream velocity, mm/s
$\underline{V}$ = local velocity vector, mm/s
V_θ = swirl velocity (time mean) of incident vortex, mm/s
x = streamwise coordinate, mm
x_p = distance from leading edge of plate, mm
y = cross-stream coordinate, mm
z = spanwise coordinate, mm
α = angle of attack, (rad)
Γ = circulation, $\int \underline{V} \cdot d\underline{r}$, mm^2/s
η = variable of integration in y direction, mm
ξ = variable of integration in x direction, mm
ζ = variable of integration in z direction, mm
ω = frequency, $2\pi f$, rad/s
$\underline{\omega}$ = three-dimensional vorticity vector, 1/s
ω_i = component of vorticity in i direction, 1/s
$\langle F \rangle_{sp}$ = spatially averaged value of F
$(\,)_i$ = quantity evaluated in i direction, where i is x, y, or z

I. Introduction

THE impingement of streamwise-oriented vortices on aerodynamic appendages such as fins and tails can result in severe loading and vibration. Over the past decade, a number of studies have addressed this phenomenon. Lee and Tang,[1] Lee et al.,[2,3] Shah,[4] Shah et al.,[5] Washburn et al.,[6] Hebbar et al.,[7] and Bean and Wood[8] have focused on measurement of the unsteady surface pressure and acceleration, aided by qualitative flow visualization, principally in the region upstream of the vortex-tail encounter. Recent quantitative velocity measurements of Lee et al.[9] at locations upstream of the vortex-tail encounter show that the burst vortex flow on a model F/A-18 aircraft has similar characteristics as that on a standard delta wing. Visualization of the burst vortices in a crossflow plane upstream of the vertical tails of a model F-18 aircraft (from Shah[4]) is given in Fig. 1. The encounter of each vortex with its respective tail will give rise to a highly distorted, turbulent flow pattern that, in turn, will dictate the unsteady loading. This flow distortion has remained unexplored.

A physical understanding of the interaction of vorticity fields with edges and plates is a subject of broader interest with the common theme of structural loading, vibration, and noise generation. Qualitative visualization and measurements of the unsteady loading of streamwise vortex-plate/blade interactions are described by Ham[10] and McAlister and Tung.[11] If, on the other hand, the incident vortex is oriented orthogonally to both the axis of the blade and the incident freestream, then the theoretical work of Howe[12] provides guidance. The experimental studies of Brand et al.,[13] Komerath et al.,[14] and Liou et al.[15] address vortices from helicopter blades impinging on airframes, which generate large-amplitude surface pressure fluctuations. Finally, in the event that the incident vortex is aligned with the axis of the blade, various combinations of flow visualization, vorticity, and surface pressure measurements show the consequences of vortex distortion and secondary vortex formation along the surface, as reviewed by Rockwell[16,17] and in investigations of Ziada and Rockwell,[18] Kaykayoglu and Rockwell,[19,20] Staubli and Rockwell,[21] Homa et al.,[22] and Gursul and Rockwell.[23] Many of these features have been simulated numerically in the studies of Panaras.[24,25] An assessment of the general topic of vortex-surface interactions, with emphasis on the basic mechanisms of flow separation and secondary vortex formation, is given by Doligalski et al.[26]

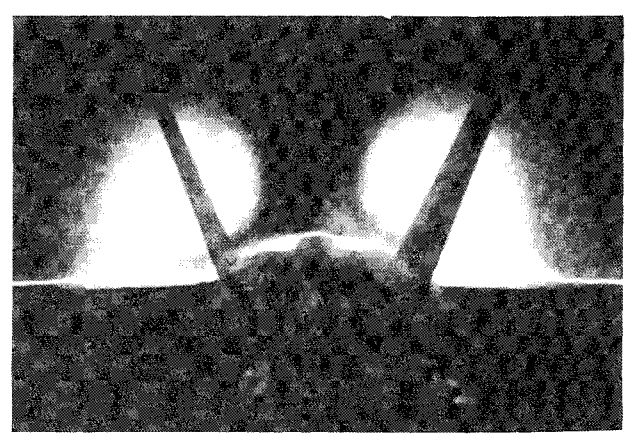

Fig. 1 Visualization of vortex breakdown upstream of vertical tails of model F-18 (from Shah[4]).

Received July 26, 1993; revision received Dec. 7, 1993; accepted for publication Dec. 13, 1993.

*Research Assistant and LASPAU Scholar, Department of Mechanical Engineering and Mechanics, 354 Packard Laboratory, 19 Memorial Drive West.

†Paul B. Reinhold Professor, Department of Mechanical Engineering and Mechanics, 354 Packard Laboratory, 19 Memorial Drive West. Member AIAA.

The objective of the present investigation is to characterize the detailed instantaneous and time-averaged structure of the encounter of a streamwise vortex in a breakdown state with a simulated tail in the form of a thin plate. High-image-density particle image velocimetry is employed to determine the streamline patterns and vorticity distributions, which lead to values of circulation, correlations, and length scales of the instantaneous concentrations of vorticity.

II. Description of Experimental System and Techniques

Figure 2a shows an overview of the experimental arrangement. A streamwise vortex was generated from the leading edge of a symmetrical delta wing. The wing was located upstream of the leading edge of the plate and oriented in a fashion such that the nominal center of the vortex intersected the leading edge. A major objective was to determine the effects of vortex breakdown on the overall vortex-plate interaction. To promote vortex breakdown at locations just upstream of the leading edge of the plate, and well upstream of the leading edge, the angle of attack of the delta wing

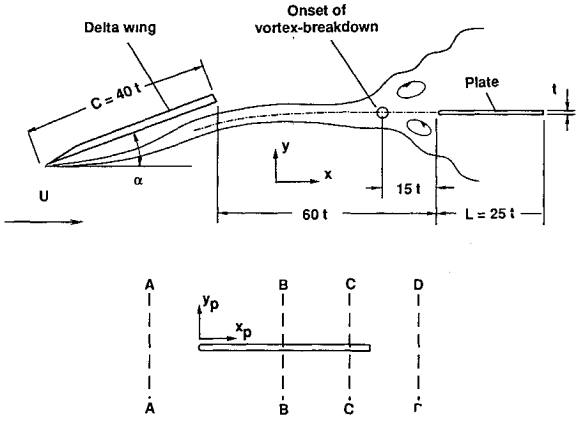

Fig. 2a Schematic of experimental arrangement.

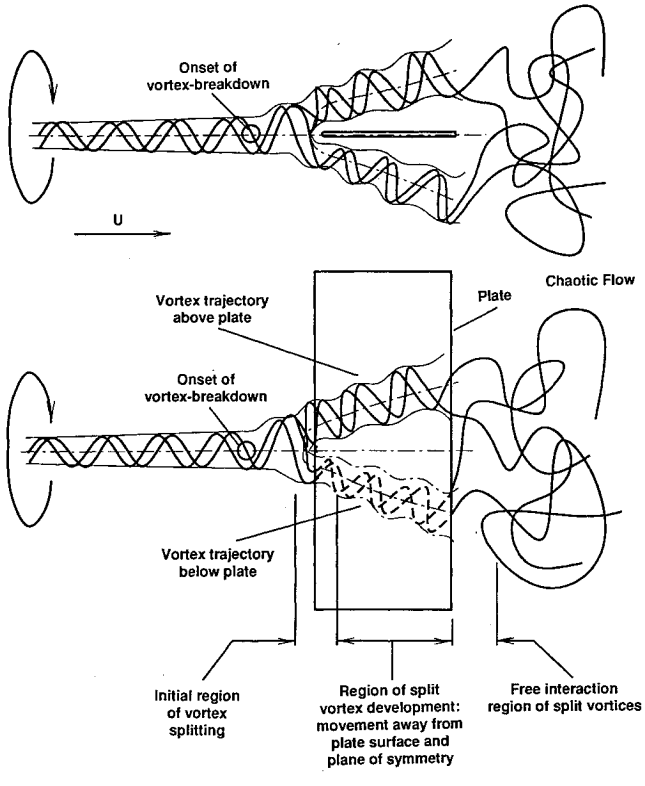

Fig. 2b Overview of principal features of vortex breakdown-plate interaction.

was adjusted to two values, α = 20 and 30 deg, respectively.[29] Unless otherwise indicated, all experimental results herein correspond to α = 20 deg.

The instantaneous structure of the flow was characterized over entire planes corresponding to end views giving streamwise vorticity ω_x and side views giving spanwise vorticity ω_z components of the three-dimensional vorticity field $\underline{\omega}$. The location of the laser sheets for the end views, indicated as A-A, B-B, and so on, are defined in the bottom schematic of Fig. 2a. These planes are located at x_p/L = –0.3, 0.5, 0.9, and 1.3, in which x_p is the streamwise coordinate from the leading edge of the plate of chord L.

The system of Fig. 2a was mounted in a large-scale water channel, having a cross section of 965 × 635 mm and a free surface water height of 533 mm. The flow velocity was maintained at 50 mm/s. The chord C of the delta wing was 240 mm, giving a Reynolds number of 9.4×10^3. The corresponding Reynolds number based on the chord L (=152 mm) of the plate was 6×10^3.

The delta wing was held in the water channel using a conventional vertical, streamlined strut fixed to the wing at its midchord. The plate was mounted horizontally between two vertical false walls made of Plexiglas. Each of these vertical walls was fixed to ends of the horizontal plate (see plan view of Fig. 2b), such that the span of the plate between the false walls was 317 mm. The height of the false walls extended above the water surface to preclude end effects. Moreover, the leading edge of the plate was located 108 mm downstream of the leading edge of the false walls. To avoid misinterpretation due to a sudden change of boundary conditions at the trailing edge of the plate, the trailing edge of the false wall arrangement extended a distance of 299 mm downstream of the trailing edge of the plate.

This arrangement also allowed forcing of the delta wing in the pitching mode to determine the effects of control of the vortex structure on the downstream vortex-plate interaction; this control was facilitated by the use of a Compumotor driving system, in turn linked to a laboratory microcomputer.

To determine the flow structure over an entire plane, a scanning version of particle image velocimetry (PIV) was employed. This technique is described by Rockwell et al.[27,28] The flow was seeded with 12-μ, metallic-coated particles. The illumination technique involved the use of a 5-W argon laser operating at a power rating from 3 to 3.5 W, directed through beam-steering focusing lenses against an oscillating mirror, as described in Mayori.[29] This approach allowed scanning frequencies of 300 Hz to be attained. At this frequency, typically three images of each particle were obtained during the shutter opening of the camera. A Nikon F-4 camera with a motor drive allowed multiple-exposure photography of the particle images. The shutter speed was set at 1/60 s. To preclude the effects of directional ambiguity, especially important when examining vortex-type flows, a bias mirror was located immediately ahead of the camera. In essence, images from the laser sheet were reflected from this mirror, which was driven to oscillate at a frequency of 12 Hz, thereby providing a positive, uniform displacement to all particle images.

The 35-mm negatives containing the particle images were interrogated using one of two techniques. In the first technique, a fringe analysis approach was employed, whereby the first Fourier transform was performed optically and the second digitally to obtain the velocity information at a specified location. The second technique was entirely digital, whereby the two successive Fourier transforms are performed on data originally digitized using a Nikon digitizer.

For both techniques, the nominal interrogation window width was 1 mm. Since the magnification of the lens for the side end views was 1:3, this gave an effective interrogation window size in the physical plane of the laser sheet of 3 mm. To satisfy the Nyquist criterion, a 50% overlap was employed during the interrogation process. That is, each successive interrogation window overlapped its neighbor by half. This provided an effective grid spacing Δl = 0.5 mm on the negative or, in the physical plane of the laser sheet, 1.5 mm. All data were subjected to a Gaussian filter with a coefficient p = 1.3. For construction of contours of constant vorticity, no additional smoothing was done. A spline fit technique

was employed to connect the contours of constant vorticity. To smooth the splines, a tension factor of 1.1 was employed.

III. Overview of Vortex-Plate Interaction

A qualitative overview of the vortex interaction process is given in Fig. 2b. It is based on quantitative PIV characterizations taken in orthogonal planes and is meant to serve as an overall guide for the detailed descriptions that follow. The onset of vortex breakdown occurs upstream of the leading edge of the plate, and the encounter of this broken-down vortex involves a vortex-splitting phenomenon whereby smaller scale vortices are generated on the upper and lower surfaces of the plate. As these split vortices are convected downstream, they move away from the plate surface and from its plane of symmetry, in the fashion illustrated. Finally, the interaction of these split vortices immediately downstream of the trailing edge of the plate generates a region of highly chaotic flow, with little evidence of the original vortical structures.

IV. Distortion of Streamwise Vorticity Field

To characterize distortion of the streamwise ω_x vorticity, views corresponding to planes A-A through D-D were employed, as defined in Fig. 2a. The overall features of the distortion process are first represented by time-averaged images; subsequently, representative instantaneous images are shown.

An overview of the time-averaged streamlines and distributions of vorticity ω_x is given in Fig. 3. These images were obtained by averaging together 10 randomly selected, instantaneous realizations. The minimum time interval between the instantaneous realizations was 2 s, corresponding to a convective time scale based on the chord L of the plate of $L/U = 3$. Upstream of the leading edge of the plate, corresponding to plane A-A, there is a single large-scale vortex. At the midchord of the plate, indicated by B-B, this vortex has undergone splitting into two smaller-scale vortices. At the trailing edge of the plate, shown in image C-C, these split vortices have moved farther away from the plane of symmetry and from the surface of the plate. There remain, however, significant concentrations of vorticity centered on the plane of symmetry, close to the surface of the plate. Finally, downstream of the trailing edge of the plate, corresponding to plane D-D, the patterns of organized streamlines and vorticity concentrations no longer exist. This sequence of interaction mechanisms with increasing streamwise distance along the plate suggests that rapid degeneration of an incident vortex is attainable through its interaction with a thin plate. During this interaction, of course, there are important mechanisms of instantaneous distortion of the flow, which act as a source of unsteady loading, i.e., buffeting, on the surface. It is therefore important to determine the instantaneous structure, which can deviate substantially from the time-averaged representations of Fig. 3.

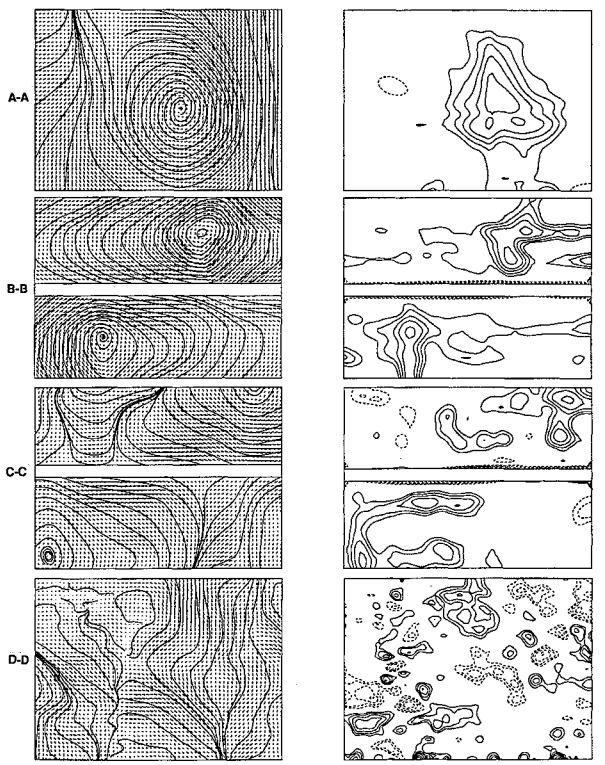

Fig. 3 Time-averaged images of streamlines and contours of constant vorticity ω_x in various crossflow planes: A-A (upstream of leading edge of plate), B-B (at midchord of plate), C-C (at trailing edge of plate), and D-D (downstream of plate). Positive and negative ω_x represented by solid and dashed lines, respectively.

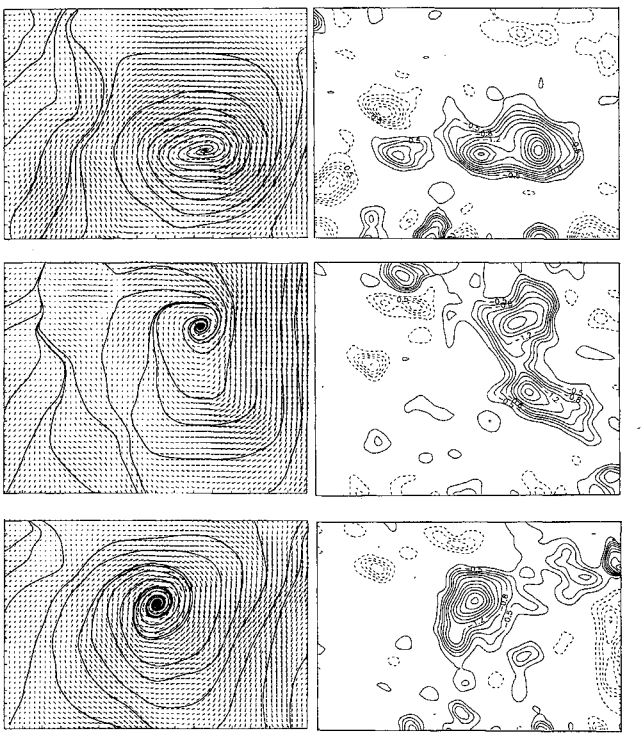

Fig. 4 Instantaneous patterns of streamlines and contours of constant streamwise vorticity ω_x in plane A-A located upstream of plate. Positive and negative ω_x represented by solid and dashed lines, respectively.

Instantaneous images of the vortex cross section before its encounter with the plate (A-A) are given in Fig. 4. The instantaneous streamline patterns in the left column show that not only the apparent location of the center of the vortex but also its pattern of rollup varies substantially from one instant to the next. In fact, close inspection of the streamline rollup and the corresponding direction of the velocity vectors shows that the vortices in all three cases correspond to an inward-spiraling motion. From the standpoint of flow topology, as addressed by Perry and Steiner,[30] this means that the incident vortex is not only highly three dimensional but is undergoing stretching along its axis. Considering the corresponding concentrations of vorticity in the right column of Fig. 4, it is evident from cross comparison with the streamline patterns that the incident vortex consists not simply of a single large-scale concentration but of several well-defined concentrations of vorticity, due to the onset of vortex breakdown upstream of the leading edge. Obviously, these changes of the vorticity concentrations with time will produce highly unsteady loading of the leading-edge region in contrast to that suggested by the time-averaged representation of the incident vortex (plane A-A) depicted in Fig. 3.

Instantaneous details of the vortex splitting are indicated in Fig. 5. The instantaneous streamline patterns on the upper and lower surfaces of the plate indicate substantially different forms from one instant to the next. Examinations of the patterns of streamline rollup and the direction of the velocity vectors show that either an inward or outward spiral occurs, depending on the particular instant of time; this corresponds to local stretching or contraction of the

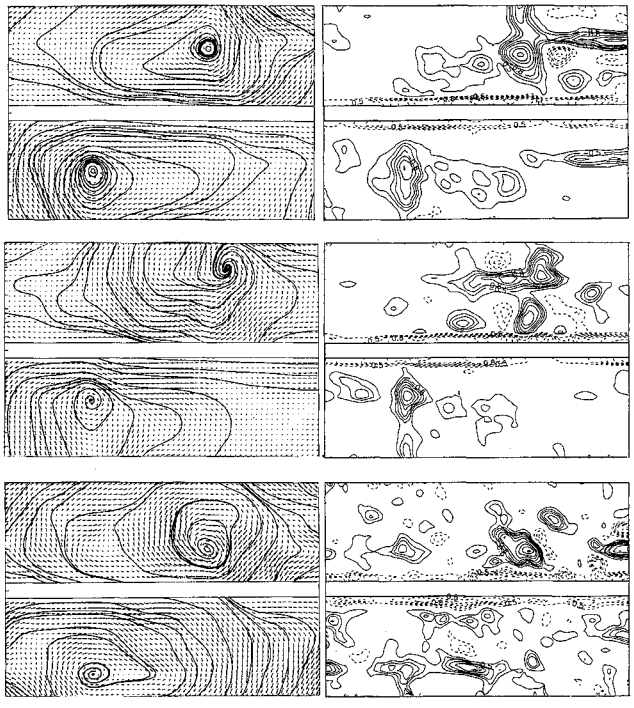

Fig. 5 Instantaneous patterns of streamlines and contours of constant vorticity in plane B-B located at midchord of plate. Positive and negative ω_x represented by solid and dashed lines, respectively.

longitudinally oriented concentrations in the vicinity of the center (foci) of the streamline rollups. Comparing the streamline patterns with the corresponding concentrations of positive (solid lines) and negative (dashed lines) vorticity in Fig. 5, it is evident that the pattern of a single vortex suggested by the streamline rollup actually may involve several small-scale concentrations of vorticity. In other words, this process of vortex splitting can involve clusters of instantaneous streamwise ω_x vorticity that, when taken together, give the impression of a single large-scale rollup.

An overview of the patterns of instantaneous streamwise ω_x vorticity in relation to the pattern downstream of the trailing edge of the plate (plane D-D) is given in Fig. 6. This overview conveys the essence of a large number of patterns, given in Mayori.[29] Downstream of the trailing edge, the instantaneous concentrations of vorticity no longer exhibit an organized pattern. In fact, substantial concentrations of negative vorticity are interspersed among the positive concentrations.

The issue arises as to how the degree of development of the vortex breakdown process influences the basic types of mechanisms described in the foregoing. To examine this effect, the angle of attack of the delta wing was increased to $\alpha = 30$ deg, at which the onset of breakdown occurs immediately downstream of the trailing edge of the wing, i.e., well upstream of the leading edge of the plate at a distance of $55t$ from the leading edge of the plate (see Mayori[29]). This situation therefore represents an extreme case of highly evolved vortex breakdown toward a turbulent state. In this case, the streamline rollup and the concentrations of streamwise ω_x vorticity take the forms shown in plane A-A of Fig. 7. The streamline pattern does not exhibit the well-defined rollup evident in plane A-A of Fig. 6; it is associated with multiple concentrations of smaller-scale vorticity. Although intermittent vortex-splitting patterns could be detected at midchord (plane B-B), given in Mayori,[29] the most representative pattern is shown in Fig. 7. Neither the velocity field nor the vorticity contours show a well-defined splitting process. Finally, downstream of the plate corresponding to plane D-D in Fig. 7, there is no quasiorganized structure of the vorticity concentrations.

V. Distortion of Spanwise Vorticity Field

An essential feature of the process of vortex breakdown, which occurs upstream of the leading edge of the plate, is the generation of pronounced concentrations of spanwise (azimuthal) vorticity ω_z. The instantaneous structure upstream of and in the immediate vicinity of the leading edge is illustrated by the images of Fig. 8; they were randomly selected from a series taken with a spacing in time of 2 s, corresponding to $3C/U$. The criterion for selection was occurrence of a large-scale concentration of negative (dashed line) vorticity on the upper surface of the leading edge of the plate, evident in all three images of Fig. 8. Relatively large-scale concentrations of both positive and negative vorticity ω_z are evident throughout all images. If one estimates, for example, the streamwise wavelength λ between successive, large-scale concentrations of positive (solid line) vorticity, then $\lambda \sim 4$ to $5t$, where t is the thickness of the leading edge. On this basis, we expect the surface pressure fluctuations on the leading edge to be highly correlated over a distance of a least several edge thicknesses.

Unlike the case of the end view of the streamwise vortex shown in Fig. 3, averaging a number of instantaneous images of the type shown in Fig. 8 does not produce averaged, large-scale structures. This is because the large-scale structures in Fig. 8 appear at random locations from one instantaneous realization to the next. Therefore, averaging a large number of images will produce very low levels of vorticity, which have no particular meaning.

Instantaneous images taken at locations further downstream are illustrated in Figs. 9b and 9c, relative to the case of Fig. 9a. The vorticity contours of Fig. 9b indicate that the concentrations are elongated in the streamwise direction upon encounter with the plate. Correspondingly, there are substantial velocity magnitudes in a direction normal to the axis of the plate, as indicated in the corresponding images of the instantaneous velocity field. In Fig. 9c, the flow structure in the vicinity of the trailing edge takes the form of a von Kármán-like vortex street. Moreover, there is an array of vortices oriented along a line orthogonal to the axis of the von Kármán street. This array of vortices, which extends from the top to the bottom of the image, is associated with the merging of the split, vortical flows as they separate from the trailing edge (compare Fig. 2b). Although it is typically assumed that the existence of a von Kármán-like vortex street from a trailing edge is unlikely in the presence of incident turbulence of the sort

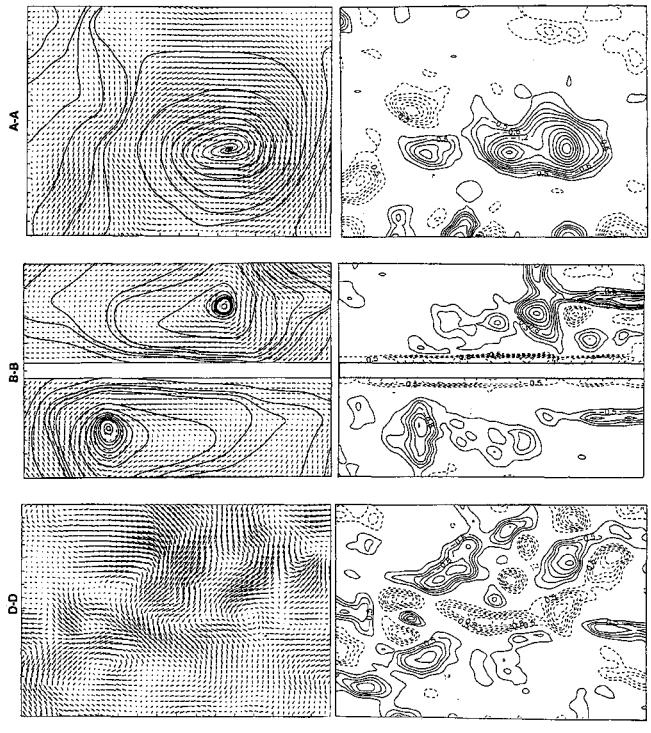

Fig. 6 Instantaneous patterns of streamlines and contours of constant streamwise vorticity ω_x in crossflow planes A-A (upstream of leading edge of plate), B-B (at midchord of plate), and D-D (downstream of trailing edge of plate). Positive and negative ω_x represented by solid and dashed lines, respectively.

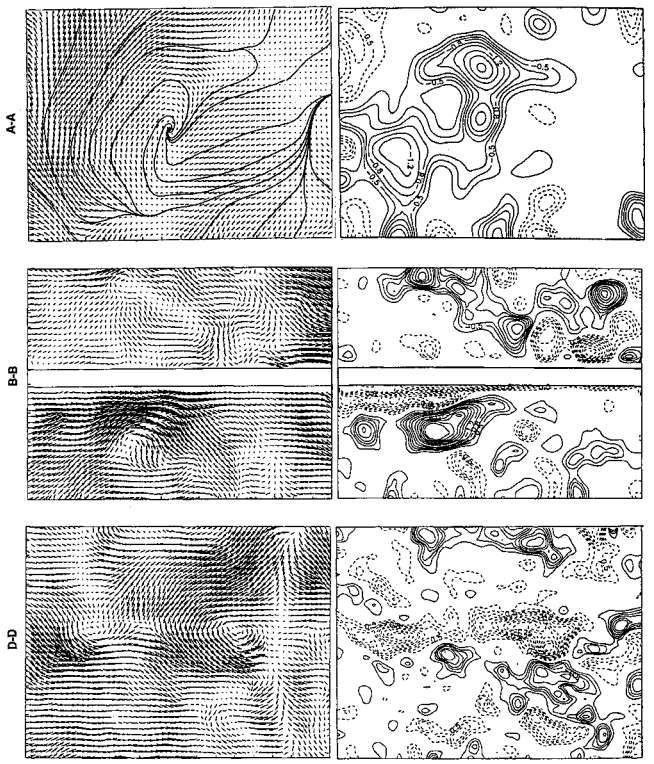

Fig. 7 Instantaneous patterns of streamlines and contours of constant streamwise vorticity ω_x in crossflow plane A-A (located upstream of leading edge of plate), B-B (at midchord of plate), and D-D (downstream of the trailing edge of the plate) for incident (broken-down) vortex generated from wing at high angle of attack $\alpha = 30$ deg. Positive and negative ω_x represented by solid and dashed lines, respectively.

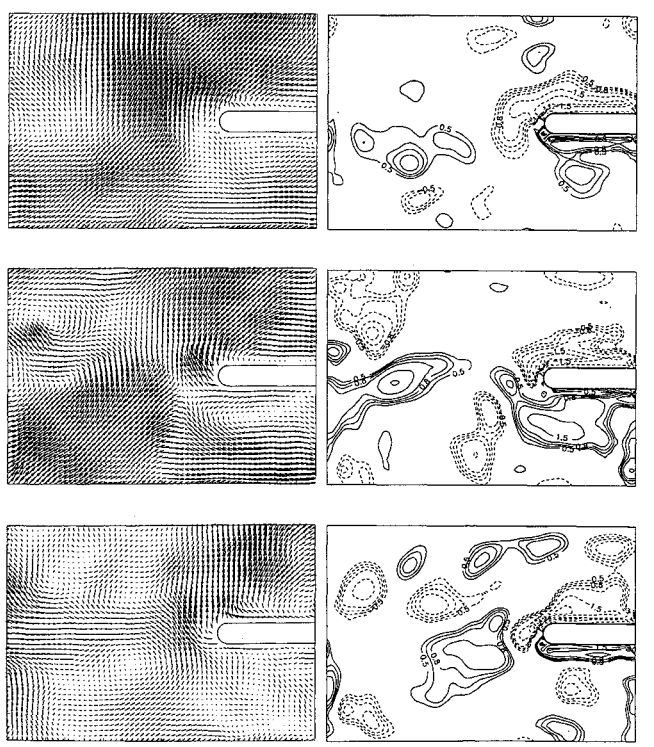

Fig. 8 Instantaneous contours of constant azimuthal vorticity ω_z at three different times in comparison with instantaneous velocity field, shown in reference frame moving at $0.9U$, where U is the average velocity over the entire image. Positive and negative ω_z represented by solid and dashed lines, respectively.

described in the foregoing, in particular that shown in Fig. 6, it is clear that this type of instability is sufficiently robust to self-generate. It persists, moreover, even in the presence of the merging of the split vortical structures and the associated instability involving the vertically oriented array of vortices.

Control of the incident vortical structures is shown in Fig. 10. Figure 10a shows the case of the streamwise vortex, in its broken-down state, interacting with the leading edge; it is formed from the stationary delta wing, as in all preceding cases. For the case of Fig. 10b, the delta wing was oscillated according to $\alpha = 20$ deg $\pm$ 2 deg sin ωt, in which $\omega = 2\pi f = 0.785$ rad/s, corresponding to a dimensionless frequency $fC/U = 0.6$. An organized pattern of small-scale vortical structures is induced. Viewing this distribution of vorticity as a whole, it is clear that the typical scale (characteristic diameter) of the vorticity concentrations has been reduced substantially relative to those of Fig. 8, where no control is applied. Now the correlation of the pressure fluctuations in the streamwise direction along the surface of the plate is directly related to the scale and wavelength of the vortical structures above the plate. Larger scales and wavelengths will produce higher correlations of surface pressure. The pressure correlations induced by the pattern of Fig. 10b are expected to be smaller than those generated by the vorticity concentrations of Fig. 8. Correspondingly, the effectiveness of the loading will be reduced. If the dimensionless frequency of oscillation is doubled relative to that of Fig. 10b, to a value of $fC/U = 1.2$ as shown in Fig. 10c, then the vortex pattern becomes substantially less organized. Moreover, the centerline of the pattern of vorticity concentrations is now displaced above the leading edge. These two effects are likely to produce broader band, lower-amplitude pressure loading on the surface, relative to that of Figs 10a and 10b.

VI. Circulation and Correlation of Vortical Structures

Figure 11 shows values of circulation Γ_x/DV_θ corresponding to time-averaged concentrations of streamwise vorticity ω_x in the crossflow plane and three-dimensional plots of vorticity correlation R_ω along with the values of the length scales L_y and L_z. Definitions of R_ω and L_y and L_z for the yz plane are as follows:

$$R_\omega = \frac{<\omega_x(y, z)\omega_x(y+n, z+\zeta)>_{sp}}{\omega_{rms}^2}$$

$$L_y = \int_0^\infty R_\omega(\eta, 0)\, d\eta$$

$$L_z = \int_0^\infty R_\omega(0, \zeta)\, d\zeta$$

Analogous expressions hold for the xy plane and the length scales L_x and L_y in that plane.

The low-level vorticity contours in each of the plots of Fig. 11 represent the complete vorticity patterns of Fig. 3. Comparing the images and values of Γ_x/DV_θ at locations A-A through D-D, it is evident that the process of vortex splitting and the eventual separation from the trailing edge of the plate produce drastic decreases in both the scale and maximum circulation of the vorticity concentrations. This observation suggests that an effective technique for attenuating vortex strength is to induce vortex splitting and subsequent interaction of the split vortices. The structure and scale of the incident and split vortex systems in Fig. 11 are reflected in the three-dimensional vorticity correlation R_ω plots, which were calculated over the domain of integration defined by the dashed lines. In plane A-A, located upstream of the encounter with the leading edge of the plate, the three-dimensional surface of R_ω drops off relatively gradually with increasing separation distances η and ζ. The vortex-splitting process, represented by the correlations R_ω at sections B-B and C-C, produces a more rapid drop-off of the R_ω surface with increasing ζ and η; in addition, there appear periodic undulations of the surface of R_ω at larger values of η and ζ. These undulations correspond to the distorted vortical structures at sections B-B and C-C; they tend to exhibit spatially periodic patterns.

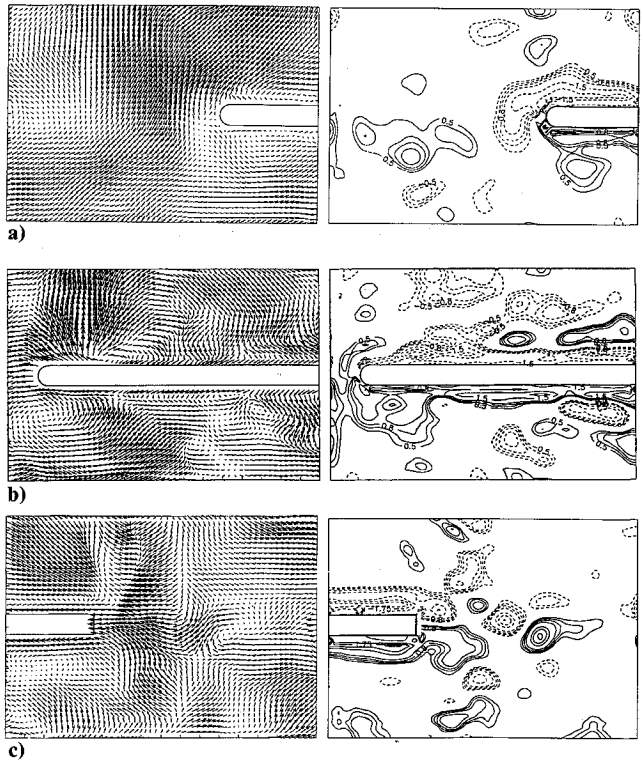

Fig 9 Instantaneous contours of azimuthal vorticity ω_z and corresponding velocity fields in a reference frame moving with 0.9U, where U is the average velocity over the entire image. Positive and negative ω_x represented by solid and dashed lines, respectively.

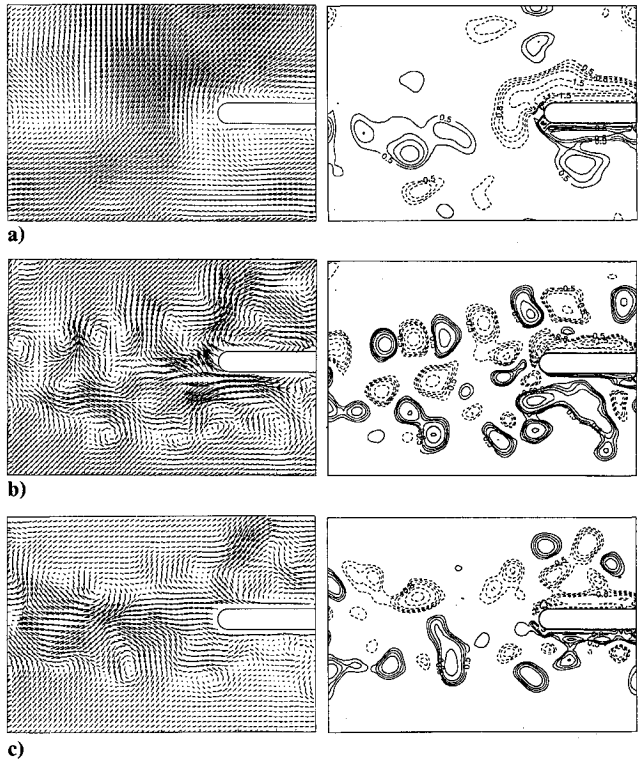

Fig. 10 Effect of controlled perturbations on structure of incident, broken-down vortex for a) no control, b) control at 0.125 Hz, and c) control at 0.25 Hz. Control is imparted by oscillating upstream delta wing with angle of attack α = 20 deg ± 2 deg sin(ωt). All vorticity contours correspond to azimuthal vorticity ω_z, and velocity fields are shown in reference frame moving with 0.9U, where U is the average velocity over the entire image. Positive and negative ω_x represented by solid and dashed lines, respectively.

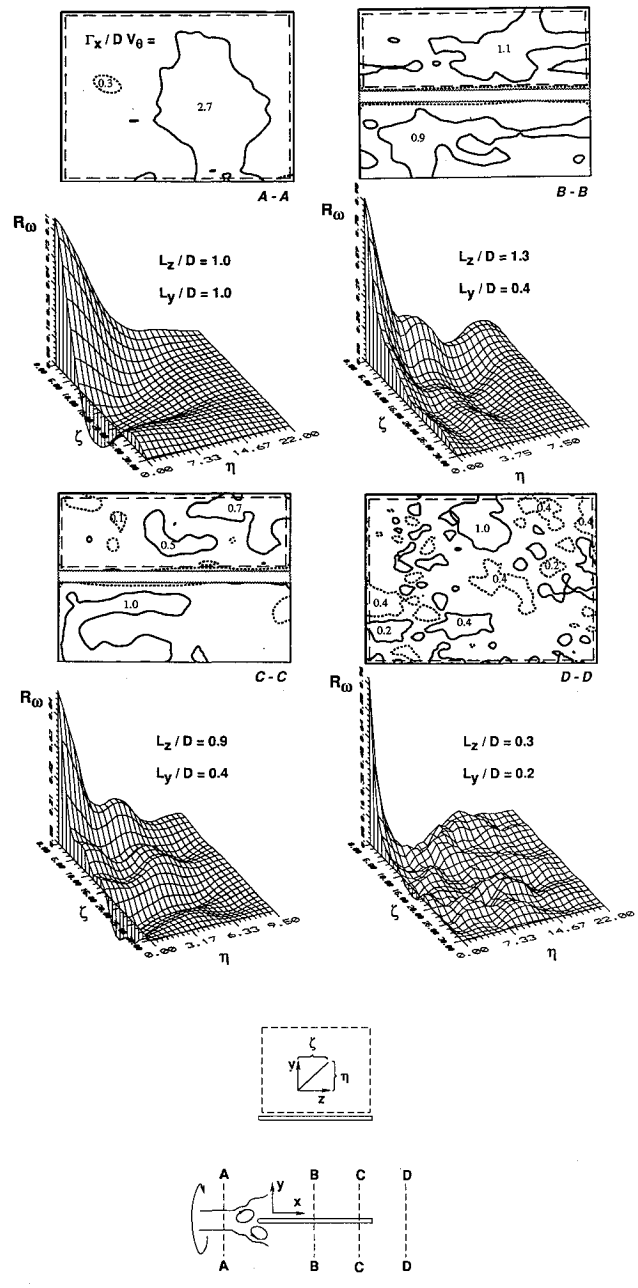

Fig. 11 Time-averaged representation of interaction in terms of contours of constant vorticity ω_x in crossflow planes A-A through D-D and corresponding vorticity correlation R_ω plots. Fields of view for evaluating R_ω are indicated by long, dashed lines. Values of circulation Γ_x and integral length scales L_y and L_z are normalized by diameter D and maximum swirl velocity V_θ of incident vortex.

Regarding the length scales L_z and L_y, comparison of their values at sections A-A through C-C shows that the process of vortex splitting induces relatively mild alterations of L_y, relative to the rather abrupt decrease in spanwise scale L_z. Immediately downstream of the trailing edge of the plate, at section D-D, the scales L_y and L_z are rapidly reduced; they have values on the order of one-third to one-fifth those of the vortex incident upon the leading edge of the plate at section A-A.

Representative patterns of the azimuthal concentrations of vorticity ω_z, values of Γ_z/DV_θ, and corresponding plots of the vorticity correlation function R_ω are given in Fig. 12; the low-level vorticity contours represent the major features of the detailed ones of Figs. 8 and 10. In general, the vortical structures immediately upstream of the leading edge of the plate have values of dimensionless circulation Γ_z/DV_θ as high as the order of 1 (Fig. 12a). On the other hand,

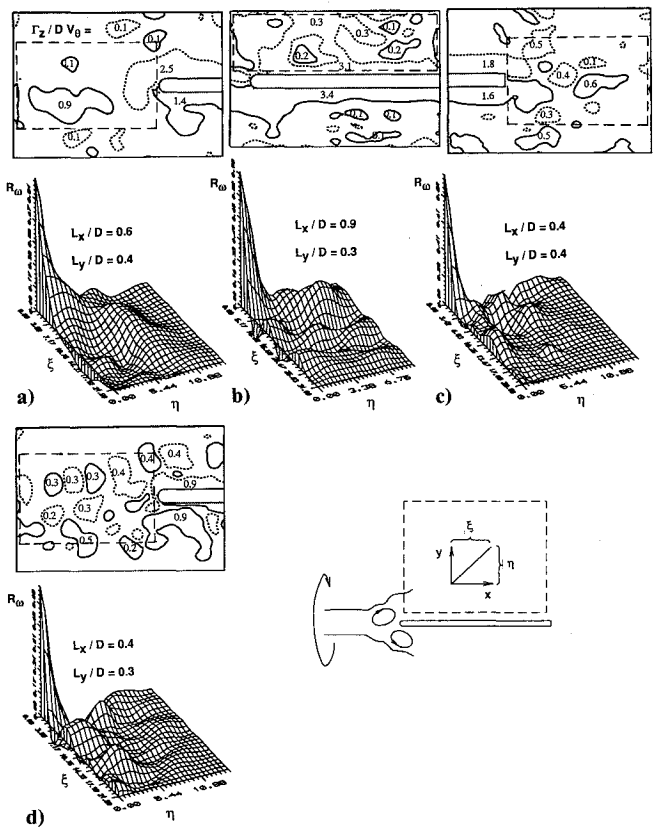

Fig. 12 Representation of vortex-plate interaction in terms of contours of constant azimuthal vorticity ω_z and corresponding vorticity correlation R_ω plots. Domains for evaluating R_ω are indicated by long, dashed lines. Values of circulation Γ_z and integral length scales L_x and L_y are normalized by diameter D and maximum swirl velocity V_θ of incident vortex.

downstream of the trailing edge of the plate (Fig. 12c), values of Γ_z/DV_θ are on the order 0.3–0.6. This trend reaffirms the process of reduction of circulation and scale of the vortices due to the interaction process with the plate, already suggested in Fig. 11. The smaller scale organized vortical structures along the plate and in the wake downstream of the trailing edge correspond to well-defined, small-scale undulations of the three-dimensional surfaces of R_ω in Figs. 12b and 12c, relative to the R_ω plot of the pre-encounter vortex of Fig. 12a. Finally, in the event that the incident vortex is controlled by oscillating the delta wing located upstream, the values of circulation and wavelength of the incident azimuthal vorticity can be reduced dramatically, relative to the noncontrolled state, evident by comparing Figs. 12d and 12a. These changes are evident in the form of the corresponding three-dimensional plot of the vorticity correlation R_ω of Fig. 12d, relative to that of Fig. 12a.

VII. Concluding Remarks

This investigation addresses the quantitative flow structure arising from interaction of a streamwise vortex in a breakdown state with a thin plate. Both the instantaneous and time-averaged structure can exhibit deterministic features, which have important consequences for the unsteady loading of the surface of the plate.

The flow patterns in the crossflow plane, in particular the contours of constant streamwise vorticity, show that the incident, broken-down vortex exhibits substantial undulations and distortions with time. Nevertheless, underlying patterns of flow structure are evident. Most importantly, the incident vortex is split into two smaller scale ones, which move away from the surface and the plane of symmetry of the plate. They encounter each other downstream of the trailing edge; however, due to the interaction of the split vortices, their identity is rapidly lost in favor of highly chaotic motion.

Regarding the concentrations of azimuthal vorticity, they are rapidly distorted as they encounter the leading edge of the plate and move downstream along its surface. Immediately downstream of the trailing edge, an embedded von Kármán vortex street is detectable. Moreover, an array of vortices oriented orthogonally to the axis of the plate is also generated; this array arises from the recombination of the split vortices near the trailing edge.

The foregoing alterations of the instantaneous and time-averaged streamwise and azimuthal vorticity distributions are characterized in terms of circulation, three-dimensional surfaces of vorticity correlation functions, and length scales of the vorticity concentrations. The circulation and length scales of the incident vortex decrease drastically due to the vortex-plate interaction.

Moreover, it is demonstrated that control of the vorticity concentrations within the incident, broken-down vortex is attainable. Substantially smaller scale vortices, relative to those occurring naturally, suggest a decreased correlation of the surface loading of the plate. Further exploration of control measures is called for, accounting for possible effects of Reynolds number on the detailed structure of the vorticity distributions.

From a practical standpoint, the details of the vortex-plate interaction process revealed here can provide a physical basis for, and serve as a preliminary guide to, the magnitude and correlation of the unsteady surface pressure field. Furthermore, the encounter process described herein occurs over a plate having a chord corresponding to only four diameters of the incident vortex, yet the vortex system is driven to a chaotic state at the trailing edge of the plate. This observation suggests that aerodynamic surfaces having small chord can be employed to mitigate larger scale, coherent vortex activity.

Further investigations will focus on the effect of sweep angle of the leading-edge thin plate in order to determine how the sweep affects the vortex encounter. Actual aircraft fin configurations must account not only for sweep angle, but also for the complex boundary conditions at the root of the fin.

Acknowledgments

The authors are pleased to acknowledge the support of the Air Force Office of Scientific Research under Grants AFOSR-91-0055 and F49620-93-1-0075, monitored by Daniel Fant.

References

[1]Lee, B. H. K., and Tang, F. C., "Buffet Load Measurements on an F/A-18 Vertical Fin High-Angle-Attack," AIAA Paper 92-2127, 1992.

[2]Lee, B. H. K., Brown, D., and Plosenski, M., "Flowfield in the Vicinity of the F/A-18 Vertical Fin at High Angle-of-Attack," *Journal of Aircraft* (to be published).

[3]Lee, B. H. K., Brown, D., Zgela, M., and Poirell, D., "Wind Tunnel Investigation and Flight Test of Tail Buffet on CF-18 Aircraft," AGARD CP-483, 1990.

[4]Shah, G. H., "Wind-Tunnel Investigation of Aerodynamic Tail Buffet Characteristics of Leading-Edge Extension Modifications to the F/A-18," AIAA Paper 91-2889, Aug. 1991.

[5]Shah, G. H., Grafton, S. B., Guynn, M. D., Brandon, J. M., Dansberry, B. E., and Patel, S. R., "Effect of Vortex Flow Characteristics on Tail Buffet and High-Angle-of-Attack Aerodynamics of a Twin-Tail Fighter Configuration," High-Angle-of Attack Technology Conference, NASA Langley Research Center, Hampton, VA, Oct. 1990.

[6]Washburn, A. E., Jenkins, L. N., and Ferman, M. A., "Experimental Investigation of Vortex-Fin Interaction," AIAA Paper 93-0050, Jan. 1993.

[7]Hebbar, S., Platzer, N., and Frink, W., "Vortex Wake Investigation of a Twin-Tail," AIAA Paper 93-0868, Jan. 1993.

[8]Bean, D. E., and Wood, M. J., "An Experimental Investigation of Twin Fin Buffeting and Suppression," AIAA Paper 93-0054, Jan. 1993.

[9]Lee, J. W., Cavone, A. A., and Suzuki, K. E., "Doppler Global Velocimetry Measurements of the Vortical Flow Above a F/A-18," AIAA Paper 93-0414, Jan. 1993.

[10]Ham, M. D., "Some Preliminary Results from an Investigation of Blade-Vortex Interaction," *American Helicopter Society Journal*, Vol. 20, No. 4, 1975, pp. 26–31.

[11]McAlister, K. W., and Tung, C., "Airfoil Interaction with an Impinging Vortex," NASA TP 2273, 1984; AVSCOM TR 83-A-17, Feb. 1984.

[12]Howe, M. S., "Unsteady Forces and Sound Produced by Normal Chopping of a Rectilinear Vortex," *Journal of Fluid Mechanics*, Vol. 6, 1989, pp. 131–153.

[13]Brand, A. G., McMahon, H. M., and Komerath, N. M., "Surface Pressure Measurements on a Body Subject to Vortex Wake Interaction," *AIAA Journal,* Vol. 27, No. 5, 1989, pp. 569–574.

[14]Komerath, N. M., Kim, J. M., and Lion, S. G., "Interaction Between a Vortex Dominated Wake and a Separated Flow Field," AIAA Paper 91-1819, June 1991.

[15]Liou, S. G., Komerath, N. M., and McMahon, H. M., "Measurement of the Interaction Between a Rotor Tip Vortex and a Cylinder," *AIAA Journal,* Vol. 28, No. 6, 1990, pp. 975–981.

[16]Rockwell, D., "Invited Lecture: Oscillations of Impinging Shear Layers," *AIAA Journal,* Vol. 21, No. 5, 1983, pp. 645–664.

[17]Rockwell, D., "Unsteady Loading of Leading-Edges in Unstable Flow—An Overview" AIAA Paper 84-2306, Oct. 1984.

[18]Ziada, S., and Rockwell, D., "Vortex-Leading-Edge Interaction," *Journal of Fluid Mechanics,* Vol. 118, 1982, pp. 79–107.

[19]Kaykayoglu, R., and Rockwell, D., "Vortices Incident Upon a Leading-Edge: Instantaneous Pressure Fields," *Journal of Fluid Mechanics,* Vol. 156, 1985, pp. 439–461.

[20]Kaykayoglu, R., and Rockwell, D., "Unstable Jet-Edge Interaction. Part I—Instantaneous Pressure Fields at a Single Frequency," and "Unstable Jet-Edge Interaction. Part II—Multiple Frequency Pressure Fields," *Journal of Fluid Mechanics,* Vol. 169, 1986, pp. 125–172.

[21]Staubli, T., and Rockwell, D., "Interaction of an Unstable Planar Jet with an Oscillating Leading-Edge," *Journal of Fluid Mechanics,* Vol. 176, 1987, pp. 135–167.

[22]Homa, J., Lucas, M., and Rockwell, D., "Interaction of Impulsively-Generated Vortex Pairs with Bodies," *Journal of Fluid Mechanics,* Vol. 197, 1990, pp. 571–594.

[23]Gursul, I., and Rockwell, D., "Vortex Street Impinging Upon an Elliptical Leading-Edge," *Journal of Fluid Mechanics,* Vol. 211, 1990, pp. 211–241.

[24]Panaras, A. G., "Pressure Pulses Generated by the Interaction of a Discrete Vortex with an Edge," *Journal of Fluid Mechanics,* Vol. 154, 1985, pp. 445–461.

[25]Panaras, A. G., "Numerical Modeling of the Vortex-Airfoil Interaction," *AIAA Journal,* Vol. 25, No. 1, 1987, pp. 5–11.

[26]Doligalski, T., Smith, C. R., and Walker, J. D. A., "Vortex Interactions with Walls," *Annual Review of Fluid Mechanics* (to be published).

[27]Rockwell, D., Magness, C., Towfighi, J., Akin, O., and Corcoran, T., "High-Image Density PIV Using Laser Scanning Techniques," *Experiments in Fluids,* Vol. 14, 1993, pp. 181–192.

[28]Rockwell, D., Magness, C., Robinson, O., Towfighi, J., Akin, O., Gu, W., and Corcoran, T., "Instantaneous Structure of Unsteady Separated Flows via Particle Image Velocimetry," Fluid Mechanics Laboratories, Dept. of Mechanical Engineering and Mechanics, Lehigh University, Rept. PI-1, Bethlehem, PA, Feb. 1992.

[29]Mayori, A., "Interaction of a Streamwise Vortical Flow with a Plate," M. S. Thesis, Dept. of Mechanical Engineering and Mechanics, Lehigh Univ., Bethlehem, PA, April 1993.

[30]Perry, A. E., and Steiner, T. R., "Large-Scale Vortex Structures in Turbulent Wakes Behind Bluff Bodies. Part 1. Vortex Formation," *Journal of Fluid Mechanics,* Vol. 174, 1987, pp. 233–270.